



A new soil roughness parameter for the modelling of radar backscattering over bare soil

Mehrez Zribi, Azza Gorraeb, Nicolas Baghdadi

► To cite this version:

Mehrez Zribi, Azza Gorraeb, Nicolas Baghdadi. A new soil roughness parameter for the modelling of radar backscattering over bare soil. *Remote Sensing of Environment*, 2014, 152 (152), pp.62-73. 10.1016/j.rse.2014.05.009 . hal-01016246

HAL Id: hal-01016246

<https://hal.science/hal-01016246>

Submitted on 29 Jun 2014

HAL is a multi-disciplinary open access archive for the deposit and dissemination of scientific research documents, whether they are published or not. The documents may come from teaching and research institutions in France or abroad, or from public or private research centers.

L'archive ouverte pluridisciplinaire **HAL**, est destinée au dépôt et à la diffusion de documents scientifiques de niveau recherche, publiés ou non, émanant des établissements d'enseignement et de recherche français ou étrangers, des laboratoires publics ou privés.

A new soil roughness parameter for the modelling of radar backscattering over bare soil

M. Zribi^a, A. Gorraeb^{a-b} and N. Baghdadi^c

^aCESBIO (CNRS/UPS/IRD/CNES), 18 av. Edouard Belin, bpi 2801, 31401 Toulouse cedex9, France

^bINAT/LRSTE (Université de Carthage), 43 av. Charles Nicolle 1082, Tunis, Mahrajène Tunisie

^cIRSTEA, UMR TETIS, 500 rue François Breton, 34093 Montpellier cedex 5, France

Abstract

The characterisation of soil surface roughness is a key requirement for the correct analysis of radar backscattering behaviour. It is noteworthy that an increase in the number of surface roughness parameters in a model also increases the difficulty with which data can be inverted for the purposes of estimating soil parameters. In this paper, a new description of soil surface roughness is proposed for microwave applications. This is based on an original roughness parameter, Z_g , which combines the three most commonly used soil parameters: root mean surface height, correlation length, and correlation function shape, into just one parameter. Numerical modelling, based on the moment method and integral equations, is used to evaluate the relevance of this approach. It is applied over a broad dataset of numerically generated surfaces characterised by a large range of surface roughness parameters. A strong correlation is observed between this new parameter and the radar backscattering simulations, for the HH and VV polarizations in the C and X bands. It is proposed to validate this approach using data acquired in the C and X bands, at several agricultural sites in France. It was found that the parameter Z_g has a high potential for the analysis of surface roughness using radar

measurements. An empirical model is proposed for the simulation of backscattered radar signals over bare soil.

Keywords: Soil, Roughness, Moisture, Zg, Radar, Backscattering coefficient, Model

1. Introduction

Soil moisture and roughness parameters play a key role in hydrological and climate studies. In recent years, various efforts have been devoted to the analysis of the backscattering characteristics of bare soils. Initially, different backscattering models (theoretical, semi-empirical and empirical) were developed (Ulaby et al., 1986, Fung et al., 1992, Oh et al., 1992, Dubois et al., 1995, Chen et al., 2003, Zribi et al., 2008). More recently, several studies have proposed various approaches for the improvement of roughness descriptions (Oh et al., 1998, Mattia et al., 1999, Zribi et al., 2000, Davison et al., 2000, Li et al., 2002, Callens et al., 2006, Verhoest et al., 2008, Bretard et al., 2013), which are essential to the accurate analysis and interpretation of backscattering behaviour and soil moisture estimation (Lievens et al., 2009). An analysis based on a fractal representation has been proposed (Rouvier et al., 1997; Zribi et al., 2000) allowing a multi-scale description, which is not limited to the use of a single scale based on the correlation length parameter. Zribi et al. (2000) introduced fractal and Brownian approaches to describe the correlation function, whereas Li et al. (2002) proposed a general power law description of roughness spectra. Fung et al. (1994), Shi et al. (1997) and Zribi et al. (2005) have proposed different types of analytical correlation function, used to fit the experimental data. Although all of these studies have led to improvements in the direct backscattering simulations, the availability of a limited number of radar configurations makes it generally impossible to retrieve the volumetric soil moisture with all of the roughness parameters. In this context, Zribi and Dechambre (2003) introduced a description based on the parameter $Zs = s^2/l$, where s is the rms surface height and l is the

correlation length (Bretard et al., 2013, Lawrence et al., 2013). Baghdadi et al. (2004, 2006, 2011) proposed an empirical correlation length, computed as a function of the rms height, radar frequency, incidence angle and polarization, in order to obtain a better fit between Integral Equation Model (Fung et al., 1992) simulations and radar observations. Lievens et al. (2011) show that roughness parameters differ between SAR acquisitions, as they are related to the observed backscatter coefficients and variations in local incidence angle. A statistical model was thus developed, to allow the effective roughness parameters to be estimated from microwave backscattering observations. Despite these contributions, the influence of roughness is still poorly modelled in currently known inversion techniques.

In the present study, a new surface description is proposed, in which the analysis uses the moment method to numerically simulate the backscattering integral equations. Our paper is organised into five sections, of which Section 2 presents the principles of the numerical backscattering simulations, Section 3 discusses the influence of roughness on the backscattering simulations and introduces the new roughness parameter, Z_g . Section 4 describes the potential of this parameter, through the use of experimental analyses based on different types of ground and radar measurements. Finally, our conclusions are presented in Section 5.

2. Numerical backscattering simulations - methodology

A numerical backscattering model based on the moment method is used to simulate radar signals over bare soils (Harrington, 1968, Chen et al., 1990, Johnson et al., 1996, Mattia et al., 2000, Soriano et al., 2002, Zribi et al., 2010). With this approach, the computations are made using simulated surfaces, with various roughness and soil moisture characteristics. The first step in this process thus involves the generation of soil roughness profiles.

2.1 Roughness profile generation for different types of correlation function

In this section, it is proposed to generate soil surfaces with different correlation functions

$$\rho(x) = \exp\left[-\left(\frac{x}{l}\right)^\alpha\right], \text{ in which the parameter } \alpha \text{ can range between 1 and 2 (Li et al., 2002),}$$

with these extremes corresponding to exponential and Gaussian functions, respectively (Fung et al., 1985). The approach described by (Fung et al, 1985) is used as follows:

The surface heights are written as:

$$h(k) = \sum_{i=-M}^{i=M} W(i)X(i+k) \quad (1)$$

where $X(i)$ is a Gaussian random variable $N(0,1)$, and $W(i)$ is the weighting function given by

$W(i) = F^{-1}\left[\sqrt{F[C(i)]}\right]$, in which $C(i)$ is the correlation function and $F[]$ denotes the Fourier transform operator. In the numerical simulations, a Fast Fourier Transformation (FFT) is used to compute the corresponding values of $W(i)$.

Fig. 1 shows three soil profiles generated using different values of α ($\alpha=1$, $\alpha=1.5$ and $\alpha=2$). In this case, the rms surface height is equal to 0.6 cm and the correlation length is equal to 6 cm. It can be clearly seen that a decrease in the value of α leads to an increase in the presence of high frequency structures.

892.2 Moment Method simulations

In this section, a limited description of the moment method, used to compute radar backscattering over generated surfaces, is proposed. The analyses presented here make use of two-dimensional simulations, which are adequate for the purposes of the present study, and are based on the use of isotropic surfaces only (Chen et al., 1994, Fung, 1994). The backscattering computation is based on the numerical resolution of integral equations, in which the medium is considered to be air (Chen et al., 1990):

$$\vec{n} \times \vec{E}^i(\vec{r}) = -\frac{1}{2} \vec{K} + \vec{n} \times \int_c \left[j\omega\mu_0 G_1 \vec{J} - \vec{K} \times \nabla G_1 - \frac{\nabla' \cdot \vec{J}}{j\omega\epsilon_1} \nabla G_1 \right] dl' \quad (2)$$

$$\vec{n} \times \vec{H}^i(\vec{r}) = -\frac{1}{2} \vec{J} + \vec{n} \times \int_c \left[j\omega\epsilon_1 G_1 \vec{K} + \vec{J} \times \nabla G_1 - \frac{\nabla' \cdot \vec{K}}{j\omega\mu_0} \nabla G_1 \right] dl' \quad (2)$$

When the medium is soil rather than air, the corresponding integral equations are:

$$0 = -\frac{1}{2} \vec{K} - \vec{n} \times \int_c \left[j\omega\mu_0 G_2 \vec{J} - \vec{K} \times \nabla G_2 - \frac{\nabla' \cdot \vec{K}}{j\omega\epsilon_2} \nabla G_2 \right] dl'$$

$$0 = -\frac{1}{2} \vec{J} - \vec{n} \times \int_c \left[j\omega\epsilon_0 G_2 \vec{K} + \vec{J} \times \nabla G_2 - \frac{\nabla' \cdot \vec{K}}{j\omega\epsilon_2} \nabla G_2 \right] dl' \quad (3)$$

where μ_0 is the permeability of air, ϵ_1 and ϵ_2 are the dielectric constants of air and soil, respectively, and \vec{n} is the unit outward normal to the surface. $\vec{J} = \vec{n} \times \vec{H}$ is the equivalent surface electric current density, and $\vec{K} = -\vec{n} \times \vec{E}$ is the equivalent surface magnetic current density.

The Green functions are defined in cylindrical coordinates, by the zeroth order Hankel function of the second kind, as:

$$G_i = -\frac{j}{4} H_0^{(2)}(k_i |\vec{\rho} - \vec{\rho}'|), i = 1, 2 \quad (4)$$

In this paper, we present integral equations and method of resolution only for horizontal polarisation. For vertical polarisation, the approach is similar with just minor modifications (Chen et al., 1990).

For the horizontal polarisation, the incident electric and magnetic fields are written as:

$$\vec{E}^i = -\vec{y} e^{jk_1(x \sin \theta + z \cos \theta)}$$

$$\vec{H}^i = \frac{1}{\eta} (-\vec{x} \cos \theta + \vec{z} \sin \theta) e^{jk_1(x \sin \theta + z \cos \theta)} \quad (5)$$

With $\vec{J} = \vec{y} J(l')$ and then $\nabla' \cdot \vec{J} = 0$

The integral equations could be written as:

$$\vec{n} \times \vec{E}^i(\vec{r}) = -\frac{1}{2} \vec{K} + \vec{n} \times \int_c [j\omega\mu_0 G_1 \vec{J} - \vec{K} \times \nabla G_1] dl'$$

$$0 = -\frac{1}{2} \vec{K} - \vec{n} \times \int_c [j\omega\mu_0 G_2 \vec{J} - \vec{K} \times \nabla G_2] dl' \quad (6)$$

where:

$$\vec{K} \times \nabla G_i = (-\vec{n}' \times \vec{E}) \times \nabla G_i = -\vec{E} (\vec{n}' \cdot \nabla G_i), \quad i = 1, 2$$

The integral equations can then be simplified to:

$$E_y^i(\vec{\rho}) = \frac{1}{2} E_y(\vec{\rho}) + \int_c [j\omega\mu_0 G_1 J_y + E_y(\vec{n}' \cdot \nabla G_1)] dl'$$

$$0 = \frac{1}{2} E_y(\vec{\rho}) - \int_c [j\omega\mu_0 G_2 J_y + E_y(\vec{n}' \cdot \nabla G_2)] dl' \quad (7)$$

These equations can then be rewritten in the form of a matrix system:

$$\begin{bmatrix} Q^{11} & Q^{12} \\ Q^{21} & Q^{22} \end{bmatrix} \begin{bmatrix} E_y \\ J_y \end{bmatrix} = \begin{bmatrix} E_y^i \\ 0 \end{bmatrix} \quad (8)$$

The details of the different terms in these matrices are described in (Chen et al., 1989).

The solution for this system allows the electric field and electric field density to be estimated over the studied surface. The backscattered field can then computed as:

$$E_y^s = - \int_c \left[j\omega \mu_0 G_1 J_y + E_y (\vec{n}' \cdot \nabla G_1) \right] dl' \quad (9)$$

This leads to the following expression for the backscattered signal:

$$\sigma^0 = \frac{2\pi\rho}{PL_{eff}} \left[\sum_{j=1}^P |E_j^s|^2 - \frac{1}{P} \left| \sum_{j=1}^P E_j^s \right|^2 \right] \quad (10)$$

Where L_{eff} is the effective illumination length of Gaussian antenna pattern.

On the basis of the outcome of several convergence tests, the profile length was set to 1 m and the number of profiles as taken to be 100. For each profile, the size of the cells was taken to be $\lambda/10$, where λ is the wavelength of the radar signal.

3. Analysis of simulated radar backscattering as a function of roughness

3.1 Influence of roughness on the backscattering simulations

In order to study the influence of the soil roughness parameters on radar signal backscattering, Moment Method (MM) simulations were run in the HH and VV polarizations, at 20 and 40° incidence angles, and at three different values of soil moisture: 10%, 20% and 30%. The results shown in Figs. 2, 3, 4 and 5 were computed at a 40° incidence angle, since the radar signals are known to be more sensitive to roughness at higher incidence angles (Fung, 1994, Zribi et al., 1997). Various surface parameters were used: rms heights $s=0.4$ cm, $s=0.6$ cm, $s=0.8$ cm, $s=1$ cm, $s=1.2$ cm, $s=1.4$ cm, $s=1.6$ cm; correlation lengths $l=4$ cm, $l=6$ cm, $l=8$ cm and $l=10$ cm; α parameter $\alpha=1$, $\alpha=1.25$, $\alpha=1.5$ and $\alpha=1.75$. The latter range (for the parameter α) was based on the values retrieved during various experimental campaigns (Zribi et al., 2005).

Fig. 2 shows the simulated backscattered signal, for the *HH* polarization, assuming volumetric moisture conditions of 10% and 30% in the C and X bands at 40° incidence, for all of the above roughness configurations, plotted as a function of the rms surface height. These simulations show that the backscattered signal is moderately well correlated with the rms surface height (in the C band, R^2 is equal to 0.65 and 0.66, and in the X band it is equal to 0.58 and 0.51, for volumetric moistures of 10% and 30%, respectively). This outcome is influenced, in particular, by the correlation length, which is not taken into account in the above relationships. Fig. 3 plots the simulated backscattered radar signals for the *HH* polarization, for volumetric moistures of 10% and 30%, in the C and X bands at 40° incidence, for all of the above roughness configurations, plotted as a function of the parameter Z_s . Since the latter parameter is defined as $Z_s = s^2/l$ (Zribi and Dechambre, 2003), it combines the influence of both the soil's *rms* height and its correlation length: it is in effect given by the product of the *rms* height s , which is related to the power of the surface height variations, and the ratio s/l , which represents the local slope of the soil. The underlying motivation for the introduction of Z_s was to introduce the influence of *slope*, which is an important soil feature in the estimation of σ° . It can clearly be seen that the simulated backscattering is more strongly correlated with Z_s ($R^2 = 0.82, 0.81$ in the C band, and $R^2 = 0.71, 0.62$ in the X band, for volumetric moistures of 10% and 30%, respectively), than with the rms height. When the exponential correlation function is considered alone, the correlation between Z_s and the simulated backscattered signal is very high ($R^2 > 0.9$). When different function shapes are considered, corresponding to different values of α (1, 1.25, 1.5 and 1.75), the correlation coefficient decreases, as shown in Fig. 3. This outcome could be explained by the influence of the slope component (s/l) on backscattering, which depends on the shape of the correlation function.

3.2 Generating the Z_g parameter

172

173 The parameter Z_s was initially proposed for use with an exponential correlation (Zribi and
174 Dechambre, 2003), and weaker correlations are observed between Z_s and the simulated
175 backscattering when other correlation function shapes are considered. However, with
176 agricultural and natural soils, differing correlation function shapes are retrieved during the
177 same period. In practice, new tillage is often associated with an exponential function, whereas
178 rain-eroded and ploughed soils are often found to have correlation functions with a shape
179 lying between that of an exponential and a Gaussian function (Zribi et al., 1997, Zribi et al.,
180 2005). For these reasons, the use of a single roughness parameter, with an rms height,
181 correlation length and correlation function shape, could be very useful for inversion studies
182 based on the analysis of radar measurements, which generally make use of a small number of
183 radar configurations.

184 Since the contribution of the ratio s/l must be different from one correlation shape to another,
185 as a result of differences in the high frequency spectrum of the soil profile, we propose to
186 introduce a new parameter, which is a global representation of the Z_s parameter, written as:

$$187 \quad Z_g = s \cdot \left(\frac{s}{l} \right)^{g(\alpha)} \quad (11)$$

188

189 where $g(\alpha)$ is a power function accounting for the influence of the ratio (s/l) on Z_g , and α is
190 the power of the correlation function.

191 In the following, it is assumed that $g(\alpha)$ can be written as:

$$192 \quad g(\alpha) = a \alpha + b$$

193 where a and b are constants.

194 All of the backscattering simulations made in the C- and X- bands, using three values of
195 volumetric moisture (10%, 20% and 30%), a large range of values of rms height (from 0.4 to
196 1.6 cm), correlation length (from 4 cm to 10 cm), and α (from 1 to 1.75), were reviewed. The

best correlation between the global roughness parameter Z_g and the simulations was determined by least squares regression. This is obtained when the function g is written as:

$$g(\alpha) \approx \alpha \quad (12)$$

such that (from Eq. 11):

$$Z_g = s \left(\frac{s}{l} \right)^\alpha \quad (13)$$

In Zribi and Dechambre (2003), it was proposed to use a roughness parameter $Z_s = (s.s/l)$, in the case of simulations corresponding to the special case of an exponential correlation function ($\alpha=1$).

For a fixed value of α , small values of Z_g correspond to small values of s and/or large values of l , whereas large values of Z_g correspond to large values of s or small values of l . In the case of a fixed correlation length, small values of Z_g correspond to small values of s and/or large values of α , whereas large values of Z_g correspond to large values of s or small values of α . A smooth soil surface (without clods) is generally characterised by a small value of s and a medium to large value of l , thus to a small value of Z_g . Ploughed soil, corresponding to new tillage, is generally associated with a large value of s , a medium to large value of l , and a value of α close to 1, and thus to a large value of Z_g . Ploughed surfaces, corresponding to eroded soils, are often characterised by a large value of s , a medium to large value of l and a value of α close to 2, thus to a medium value of Z_g . Even when its *rms* height (s) is small, a cloddy soil is characterised by a very small value of l and a value of α close to 1, thus leading to large values of Z_g (Zribi et al., 1997, zribi et al., 2005).

Fig. 4 shows a plot of simulated backscattered signals as a function of Z_g , for various ranges of roughness and four correlation function shapes ($\alpha=1$, $\alpha=1.25$, $\alpha=1.5$, $\alpha=1.75$), in the C and X bands and for the *HH* polarization, with volumetric moisture values of 10% and 30%.

Firstly, it can be seen that the simulated backscattering increases with Z_g , and that there is a strong correlation between the backscattering and Z_g , equal to 0.97 and 0.97 for 10% and 30% volumetric moistures in the C-band and equal to 0.97 and 0.93 for 10% and 30% volumetric moistures in the X-band. A high dynamic range can be observed at small values of Z_g , and near saturation can be seen when Z_g reaches approximately 0.3-0.35. The highest values of α produce the weakest backscattering. From this initial result, Z_g appears to be a useful parameter for the characterization of surface roughness, in the case of a given (fixed) radar configuration. This result can be explained by the fact that Z_g takes the influence on radar backscattering behaviour of s , l and the correlation function shape into account.

Table 1 provides a summary of the correlations determined from backscattering simulations, using different roughness parameters (s , Z_s and Z_g), for all combined conditions of incidence angle, moisture, polarisation, and frequency. It can be seen that under almost all conditions of radar transmission, the strongest correlations are obtained with the parameter Z_g , rather than with s or Z_s . This conclusion is not completely verified in the C-band, in the case of a 20° incidence angle, for which the empirical logarithmic relationship can be seen to less well correlated.

To simplify the combination of backscattering simulations made at different radar frequencies, the former were considered as a function of electromagnetic roughness, written in the form: $k.Z_g$ (k : radar wave number). Fig. 5 plots the simulated backscattered signals as a function of $k.Z_g$, in the HH and VV polarizations, at a 40° incidence angle, and with the volumetric moisture equal to 10% and 30%, thus allowing all roughness conditions and C- and X-band simulations to be combined.

A least squares approach was then used to establish an empirical relationship between $k.Z_g$ and the backscattered signals, taking the form:

$$\sigma^0 = \alpha + \beta \left(1 - e^{-\mu k Zg} \right) \quad (14)$$

where σ^0 is expressed in dB, k in cm^{-1} , and Zg in cm.

The backscattered signals can be seen to be strongly correlated with $k.Zg$. Table 2 lists the coefficients α , β and μ , together with R^2 and the RMS error, for different moisture conditions ($M_v=10\%$, 20% and 30%), two incidence angles, 20° and 40° , and for the HH and VV polarisations. All of these configurations are characterised by a strong correlation between $k.Zg$ and the radar simulations (greater than 0.77).

4. Experimental analysis

In this study, we use data acquired over agricultural watersheds, during the course of three experimental campaigns (Orgeval'94, Pays de Caux'94, Villamblain'2003) (Fig. 6). For each of these campaigns, radar data (SIRC, ERASME, ASAR/ENVISAT) was acquired with different configurations (Table 3). Simultaneously to the radar acquisitions, ground measurements were carried out in a large number of test fields: the soil moisture was measured within the top 5 cm soil using a gravimetric method and/or a TDR probe, and roughness measurements were made using a pin-profiler (total length equal to 2 m, resolution equal to 10 mm).

4.1 Description of the database

- *Orgeval'94*

The Orgeval watershed is located to the East of Paris (France). An experimental campaign was conducted during the SIRC/XSAR mission in April 1994 (Zribi et al., 1997). The soil texture is relatively constant over the whole basin: clay 17%, silt 78%, sand 5%. Ground measurements (roughness and moisture) were made in 5 fields.

- *Pays de Caux'94*

267 This test site corresponds to the Blosseville watershed, located in the Pays de Caux in
268 Northern France (49°47' N; 0°50' W). The loamy soils of the northern European loess belt are
269 sensitive mainly to soil structure degradation, and are commonly exposed to erosion caused
270 by concentrated runoff. The site's soil is characterized by a very homogenous loamy texture
271 (13% clay, 65% loam, and 22.5% sand). ERASME FM-CW scatterometer airborne
272 measurements were recorded in 1994, over 10 large test fields.

273 • *Villamblain'2003*

274 This site is located approximately 80 km west of Paris (48°10'N; 01°48'E), and is
275 characterized by large agricultural fields, which are mainly bare soil fields with a
276 homogenous soil composed of approximately 60% loam, 30% clay and 10% sand.
277 Simultaneously to the radar measurements acquired by the ASAR-ENVISAT radar in 2003,
278 ground measurements were made over a large number of bare soil test fields.

279 • *Soil moisture measurements*

280 The mean volumetric moisture (M_v) was estimated for each test field, within the top 5 cm,
281 and using a gravimetric method. As a result of relatively rainy winters, this parameter
282 remained high and nearly constant (approximately $0.3 \text{ cm}^3/\text{cm}^3$), at all three sites.

283 • *Soil roughness measurements*

284 Roughness measurements were made using a pin profiler (with a total length of 2 m and a
285 resolution of 1 cm). Ten surface profiles were taken for each test field, in order to ensure that
286 roughness parameters were determined with sufficient statistical accuracy. For each profile,
287 we computed the correlation function (Ogilvy, 1991), as well as the two statistical parameters,
288 the rms height (s) and the correlation length (l). The parameter α , corresponding to the shape
289 of the correlation function, is computed for the first scales up to the correlation length from
290 experimental functions, using a least squares optimisation approach.

Fig. 7-a plots the parameter α , corresponding to the correlation function shapes retrieved for all test fields, as a function of the *rms* soil height, showing a moderate degree of correlation. In general, the value of α is found to be close to 1 for smooth soils, and higher for ploughed soils. This type of relationship was also observed by (Zribi et al., 2005). The measured values of Z_g (Fig.7-b) ranged between 0.01 and 0.03 for smooth soils. In the case of cloddy soils, Z_g ranged between approximately 0.04 and 0.2, and for ploughed soils it ranged between 0.2 and 0.62 (Zribi et al., 2005).

4.2 Comparing backscattering simulations with radar signal data

In Figs. 8-a and 8-b, the results derived from the moment method simulations made in two dimensions are compared with real radar data, for the *HH* and *VV* polarizations, respectively. Two-dimensional (rather than three-dimensional) simulations were used, since the analysed experimental fields had very little directional structure. For each individual test field, ground measurements (*rms* height, correlation length, α parameter, soil moisture) were used as input for the radar backscattering simulations. Fig. 8-a shows the *HH* polarization data obtained from several different configurations: C and X bands, and five different incidence angles: 20°, 25°, 30°, 35° and 44°, whereas Fig. 8-b shows *VV* polarization results for the same set of configurations. In the *HH* polarization, the simulations can be seen to deviate from the radar measurements, with an RMSE equal to 3.34 dB. In the *VV* polarization, a good agreement can be observed, with an RMSE equal to 1.62 dB. These results illustrate some of the limitations encountered, particularly in the *HH* polarization, when the MM model is used to simulate all surface conditions. This is probably due to the greater sensitivity of *HH* polarization to soil roughness (Fung, 1994, Zribi et al., 1997). In the following section, it is proposed to use empirical relationships to express the backscattered radar signals as a function of the surface parameters.

4.3 Analysis of the relationship between roughness and radar data

All of the ground data analysed in the present study was acquired under very similar soil moisture conditions (close to 30%). Fig. 9 shows the radar signals measured over the test fields, as a function of kZg , for various configurations (both polarizations and several incidence angles). As in the case of the simulations described in section 3, the radar signals are characterized by a high dynamic range at small values of kZg , and near saturation can be observed when kZg reaches approximately 0.3-0.35.

Figs. 9a, 9b, 9c, 9d, 9e, and 9f correspond to observations made at the Pays de Caux site, using the ERASME airborne FM-CW scatterometer. This data was acquired in the HH and VV polarizations, in the C-and X-bands at 20° , 25° , 30° and 35° incidence. In both polarizations, the roughness parameter kZg and the radar measurements are strongly correlated.

Fig. 9g corresponds to data acquired by SIR-C and ASAR-ENVISAT over the Orgeval and Villamblain sites, at HH polarization in the C band and an incidence of approximately 44° . These radar measurements are also found to be strongly correlated with kZg . Empirical relationships can be used to express the backscattered radar signals as a function of kZg , for various multi-incidence and polarization configurations. These are written:

$$\sigma_{p\theta}^0 = \alpha_{p\theta} + \beta_{p\theta} \left(1 - e^{-\mu_{p\theta} k Zg} \right) \quad (15)$$

where the coefficients $\alpha_{p\theta}$, $\beta_{p\theta}$ and $\mu_{p\theta}$ are adjusted using a least squares optimisation, p is the polarization and θ is the incidence angle. Table 2 lists the values of $\alpha_{p\theta}$, $\beta_{p\theta}$ and $\mu_{p\theta}$, together with the statistical parameters R^2 and RMSE, for the nine configurations analysed in this study.

Table 5 indicates the general improvement found in the statistical parameters (R^2 and RMSE) when $k.Zg$ is used, rather than $k.Zs$, in the same empirical model. Only the last configuration (HH polarization at 44°) leads to better results with the parameter $k.Zs$.

From the empirical relationships established for the nine radar configurations, a general empirical model is proposed, in which the radar signal is expressed as a function of kZg , θ and the radar polarisation:

$$\sigma_p^0 = (a_p \theta + b_p) + (c_p \theta + d_p) \times \left(1 - e^{(e_p \theta^2 + f_p \theta + g_p) k Z g} \right) \quad (16)$$

This model is found to be valid when θ lies between 20° and 44° .

The values of the parameters used in Eq. 16 are listed, for the HH and VV polarizations, in Table 6.

In Fig. 10, the radar signal levels predicted by the model are compared with the measured data, over the full range of experimental incidence angles. The modelled and measured signals are found to be strongly correlated, with R^2 equal to 0.79 and 0.88 and the $RMSE$ equal to 1.42 dB and 1.19 dB, in the HH and VV polarizations, respectively.

5. Conclusion

It is very difficult to separately estimate the influences of rms height (s), correlation length (l) and correlation function shape, on the backscattering behaviour of a rough soil surface. In practice, the availability of only a limited number of radar configurations can make it impossible to retrieve all of these parameters with soil moisture.

In the present study, a new approach is proposed for the description of surface roughness and its influence on the backscattering behaviour of radar signals. The resulting expressions make use of a numerical backscattering algorithm based on the moment method, applied to synthetically generated surfaces and assuming a correlation function described by

$$\rho(x) = \exp \left(- \left(\frac{x}{l} \right)^\alpha \right). \text{ The correlation between the simulated and measured rms soil heights is}$$

weak, as a consequence of influences related to the correlation length of the surface roughness and the shape of the correlation function. These influences must be accounted for, in order to

retrieve accurate surface roughness or moisture estimations. The parameter Z_s , which allows
 the influence of soil surface height and slope to be taken into account, can be used to improve
 the correlation strength. Nevertheless, the simulated radar signals are still affected by strong
 fluctuations, resulting from variations in the shape of the correlation function. By introducing
 a new roughness parameter (Z_g), written in the form $Z_g = s \left(\frac{s}{l} \right)^\alpha$, the influence of the *rms*
 surface height, the slope of the soil surface, and a third parameter α related to the shape of the
 correlation function, can be taken into account. A very good correlation is then observed
 between $k \cdot Z_g$ and the simulated radar signals in the C and X bands, with R^2 equal to 0.93 and
 0.9 at 40° incidence for the *HH* and *VV* polarizations, respectively. Empirical functions are
 proposed to describe these relationships. The usefulness of this new parameter is
 demonstrated through the analysis of radar signal data acquired at three experimental sites in
 France (Orgeval, Pays de Caux and Villamblain). In the case of smooth soils, Z_g is found to
 range between 0.01 and 0.03. In the case of cloddy soils, Z_g lies between approximately 0.04
 and 0.45, and in the case of ploughed soils, it ranges between 0.2 and 0.62. A high correlation
 ($R^2 > 0.7$ and $RMSE < 1.54$ dB) is observed between $k \cdot Z_g$ and the experimental radar signals
 acquired in the C and X bands, at incidence angles ranging between 20° and 44°. An
 empirical model is proposed for the relationship observed between the measured radar signals
 and $k \cdot Z_g$, θ , and the polarization parameters. This is found to be in excellent agreement with
 the radar measurements, with the $RMSE$ equal to 1.42 dB and 1.19 dB in the *HH* and *VV*
 polarizations, respectively. These results are particularly useful for the improvement of
 empirical or semi-empirical inversion models used in soil moisture estimations. In the past,
 these models were often based on the rms height roughness parameter only, leading to a high
 level of noise and a lower accuracy in the soil moisture estimation, resulting from the
 influence of the correlation length and shape of the correlation function.

Acknowledgements

388
389 This study was funded by three projects: ASCAS and CFOSAT (the TOSCA/CNES program)
390 and AMETHYST (ANR-12-TMED-0006-01). The authors wish to thank the BRGM,
391 IRSTEA and LATMOS teams for their logistical support during the field campaigns.
392

References

- Baghdadi, N., Gherboudj, I., Zribi, M., Sahebi, M., Bonn, F., and King, C. (2004). Semi-empirical calibration of the IEM backscattering model using radar images and moisture and roughness field measurements. *International Journal of Remote Sensing*, 25, 3593-3623.
- Baghdadi, N., Holah, N., and Zribi, M. (2006). Calibration of the Integral Equation Model for SAR data in C-band and HH and VV polarizations. *International Journal of Remote Sensing*, 27 (4), 805-816.
- Baghdadi, N., Abou Chaaya, J., and Zribi, M. (2011). Semi-empirical calibration of the Integral equation Model for SAR data in C-band and cross polarization using radar images and field measurements. *IEEE Geoscience and Remote Sensing Letters*, 8 (1), 14-18.
- Bretar, F., Arab-Sedze, M., Champion, J., Pierrot-Deseilligny, M., Heggy, E., Jacquemoud, S. (2013). An advanced photogrammetric method to measure surface roughness: Application to volcanic terrains in the Piton de la Fournaise, Reunion Island. *Remote Sensing of Environment*, 135, 1-11.
- Callens, M., Verhoest, N.E.C., Davidson, M.W.J. (2006). Parameterization of tillage-induced single-scale soil roughness from 4-m profiles. *IEEE Transaction on. Geoscience and Remote Sensing*. 44, 878-888.
- Chen, M. F., and Bai, S. Y. (1990). Computer simulation of wave scattering from a dielectric random surface in two dimensions cylindrical case. *J. Electromagn. Waves Appl.* 4, 10, 963-982.
- Chen, K. S., Wu, T. D., Tsang, L., Li, Q., Shi, J., and Fung, A. K. (2003). Emission of rough surfaces calculated by the integral equation method with comparison to three-dimensional moment method simulations. *IEEE Transaction on. Geoscience and Remote Sensing*, 41 (1), 90-101.
- Davidson, M. W. J., Le Toan, T., Mattia, F., Satalino, G., Manninen, T., and Borgeaud, M. (2000). On the characterisation of agricultural soil roughness for radar remote sensing studies. *IEEE Transaction on. Geoscience and Remote Sensing*, 38, 630-640.
- Dubois, P. C., Van Zyl, J., and Engman, T. (1995). Measuring soil moisture with imaging radars. *IEEE Transaction on Geoscience and Remote Sensing*, 33, 915-926.

423 Fung, A., and Chen, M. F. (1985). Numerical Simulation of Scattering from Simple and
 424 Composite Random Surfaces, *J. Opt. Am. A*, 2 (12).

425 Fung, A. K. (1994). *Microwave Scattering and Emission Models and their Applications*,
 426 Norwood: Artech House.

427 Fung, A. K., Li, Z., and Chen, K. S. (1992). Backscattering from a randomly rough dielectric
 428 surface. *IEEE Transaction on Geoscience and Remote Sensing*, 30, 356-369.

429 Harrington, R. F. (1968). Field Computation by Moment Method. IEEE PRESS, Series on
 430 Electromagnetic Waves.

431 Johnson, J. T., Tsang, L., Shin, R. T., Pak, K., Chan, C. H., Ishimaru, A., Kuga, Y. (1996).
 432 Backscattering enhancement of electromagnetic waves from two-dimensional perfectly
 433 conducting random rough surfaces: a comparison of Monte Carlo simulations with
 434 experimental data. *IEEE Transactions on Antennas and Propagation*, 44, 5.

435 Lawrence, H., Wigneron, J.-P., Demontoux, F., Mialon, A., Kerr, Y.H. (2013). Evaluating the
 436 Semiempirical H - Q Model Used to Calculate the L-Band Emissivity of a Rough Bare
 437 Soil . *IEEE Transactions on Geoscience and Remote Sensing*, 51 (7, Part: 2), 4075 –
 438 4084, Digital Object Identifier: 10.1109/TGRS.2012.2226995.

439 Li, Q., Shi, J. C., and Chen, K. S. (2002). A generalised Power Law Spectrum and its
 440 Applications to the Backscattering of soil surfaces Based on the Integral Equation
 441 Model. *IEEE Transaction on Geoscience and Remote Sensing*, 40, 271-281.

442 Lievens H., Vernieuwe H., Alvarez-Mozos J., De Baets B., Verhoest N.E.C. (2009). Error in
 443 SAR-derived soil moisture due to roughness parameterization: An analysis based on
 444 synthetical surface profiles. *Sensors*, 9(2), 1067-1093; doi:10.3390/s90201067.

445 Lievens H., Verhoest N.E.C., De Keyser E., Vernieuwe H., Matgen P., Álvarez-Mozos J., De
 446 Baets B. (2011). Effective roughness modelling as a tool for soil moisture retrieval from
 447 C- and L-band SAR. *Hydrology and Earth System Sciences*, 15(1), 151-162.

448 Mattia, F. and Le Toan, T. (1999). Backscattering properties of multi-scale rough surfaces. *J.*
 449 *Electro. Waves Appl.*, 13, 491-526.

450 Mattia, F., Le Toan, T., Davidson, M. (2001). An analytical, numerical, and experimental
 451 study of backscattering from multiscale soil surfaces. *Radio Science*, 36, 1, 119–135,
 452 DOI: 10.1029/2000RS002327

- Oh, Y., Sarabandi, K., and Ulaby, F. T. (1992). An empirical model and an inversion technique for radar scattering from bare soil surfaces. *IEEE Transactions on Geoscience and Remote Sensing*, 30, 370–381.
- Oh, Y., and Kay, Y. C. (1998). Condition for precise measurement of soil surface roughness. *IEEE Transactions on Geoscience and Remote Sensing*, 36(2), 691–695.
- Shi, J., Wang, J., Hsu, A. Y., O'Neill, P. E., and Engmann, T. (1997). Estimation of Bare Surface Soil Moisture and Surface Roughness Parameter Using L-Band SAR Image Data. *IEEE Transaction on Geoscience and Remote Sensing*, 35, 1254-1265.
- Soriano, G., Guérin, C. A., Saillard, M. (2002). Scattering by two-dimensional rough surfaces: comparison between the method of moments, Kirchhoff and small-slope approximations. *Waves Random Media*, 12, 1, 63-83, **DOI**:10.1088/0959-7174/12/1/305.
- Ulaby, F. T., Moore, R. K., and Fung, A. K. (1986). *Microwave Remote Sensing Active and Passive*. Norwood: Artech House, inc.
- Verhoest, N. E. C., Lievens, H., Wagner, W., Alvarez-Mozos, J., Moran, M. S., and Mattia, F. (2008). On the soil roughness parameterization problem in soil moisture retrieval of bare surfaces from Synthetic Aperture Radar. *Sensors*, 8 (7), 4213–4248.
- Wu, T. D., Chen, K. S., Shi, J., and Fung, A. K. (2001). A transition model for the reflection coefficient in surface scattering. *IEEE Transaction on Geoscience and Remote Sensing*, 39, 2040-2050.
- Zribi, M., Taconet, O., Le Hégarat-Masclé, S., Vidal-Madjar, D., Emblanch, C., Loumagne, C., and Normand, M. (1997). Backscattering behavior and simulation comparison over bare soils using SIRC/XSAR and ERASME 1994 data over Orgeval. *Remote Sensing of Environment*, 59, 256-266.
- Zribi, M., Ciarletti, V., and Taconet, O. (2000). Validation of a rough surface model based on fractional brownian geometry with SIRC and ERASME radar data over Orgeval site. *Remote Sensing of Environment*, 73, 65-72.
- Zribi, M. and Dechambre, M. (2003). A new empirical model to retrieve soil moisture and roughness from Radar Data. *Remote Sensing of Environment*, 84 (1), 42-52.

482 Zribi, M., Baghdadi, N., Holah, N., Fafin, O., and Guérin, C. (2005). Evaluation of a rough
483 soil surface description with ASAR-ENVISAT Radar Data. *Remote sensing of*
484 *environment*, 95, 67-76.

485 Zribi, M., André, C., Decharme, B. (2008). A method for soil moisture estimation in
486 Western Africa based on ERS Scatter meter. *IEEE Transactions on Geoscience and*
487 *Remote Sensing*, 46, 2, 438-448.

488 Zribi, M., Le Morvan, A., Dechambre, M., Baghdadi, N. (2010). Numerical backscattering
489 analysis for rough surfaces including a cloddy structure. *IEEE Transactions on*
490 *Geoscience and Remote Sensing*, 48 (5), 2367 – 2374, 10.1109/TGRS.2009.2038710.

491

Figures captions

Fig. 1: Three synthetically generated surface profiles, with *rms* height=0.6 cm, correlation length=6 cm, and a) $\alpha=1$, b) $\alpha=1.5$ and c) $\alpha=2$.

Fig. 2: Backscattering simulations in the *HH* polarisation at 40° incidence, as a function of the *rms* height: a) C band, *mv*=10%, b) C band, *mv*=30%, c) X band, *mv*=10%, d) X band, *mv*=30%

Fig. 3: Backscattering simulations in the *HH* polarisation at 40° incidence, as a function of the parameter *Zs*. a) C band, *mv*=10%, b) C band, *mv*=30%, c) X band, *mv*=10%, d) X band, *mv*=30%

Fig. 4: Backscattering simulations in the *HH* polarisation at 40° incidence as a function of the parameter *Zg*, in the parameter space defined by *s* ranging from 0.4 to 1.6cm, *l* ranging from 4 to 10 cm, and α ranging from 1 to 1.75: a) C band, *mv*=10%, b) C band, *mv*=30%, c) X band, *mv*=10%, d) X band, *mv*=30%

Fig. 5: Backscattering simulations as a function of the parameter *kZg*, at 40° incidence: a) *HH* polarization, *mv*=10%, b) *HH* polarization, *mv*=30%, c) *VV* polarization, *mv*=10%, d) *VV* polarization, *mv*=30%

Fig. 6: Map showing the location of the studied sites

Fig. 7: Roughness parameters for all test fields at the three studied sites (Orgeval, Pays de Caux, Villamblain) (a) *rms* heights and α , the power of the correlation function, (b) *rms* heights and *Zg* parameters.

Fig. 8: Numerically simulated radar signals as a function of measured radar signals, a) *HH* pol (C and X bands, at five incidence angles: 20° , 25° , 30° , 35° and 44°), (b) *VV* pol (C and X bands, at four incidence angles: 20° , 25° , 30° and 35°).

Fig. 9: Relationship between *kZg* and measured radar signals, for: a) *HH* polarization at 20° incidence, b) *VV* polarization at 20° incidence, a) *HH* polarization at 25° incidence, b) *VV*

polarization at 25° incidence, c) *HH* polarization at 30° incidence, d) *VV* polarization at 30° incidence, e) *HH* polarisation, at 35° incidence, f) *VV* polarisation at 35° incidence, g) *HH* polarisation at 44° incidence.

Fig. 10: Inter-comparison between radar data acquired at different incidence angles, and the signals given by the proposed empirical model: (a) *HH* polarization, (b) *VV* polarisation

Tables:

Table 1: The statistical parameter R^2 , computed for different backscattering simulations, as a function of the rms height (s), the parameters Z_s and Z_g , and various different values of soil moisture, incidence angle and polarisation.

configuration		$\sigma_0=f(s)$		$\sigma_0=f(Z_s)$		$\sigma_0=f(Z_g)$	
		C-band	X-band	C band	X band	C band	X band
$M_v=10\%$	HH-20°	0.77	0.53	0.89	0.66	0.9	0.95
	VV-20°	0.73	0.63	0.8	0.78	0.8	0.82
	HH-40°	0.65	0.58	0.82	0.71	0.97	0.97
	VV-40°	0.58	0.68	0.77	0.76	0.97	0.96
$M_v=20\%$	HH-20°	0.79	0.63	0.89	0.78	0.9	0.92
	VV-20°	0.58	0.66	0.89	0.8	0.81	0.86
	HH-40°	0.66	0.48	0.82	0.64	0.97	0.95
	VV-40°	0.58	0.55	0.76	0.73	0.97	0.94
$M_v=30\%$	HH-20°	0.79	0.6	0.91	0.74	0.90	0.91
	VV-20°	0.76	0.61	0.88	0.76	0.8	0.86
	HH-40°	0.66	0.51	0.81	0.62	0.97	0.93
	VV-40°	0.58	0.46	0.75	0.6	0.95	0.96

Table 2: Values of α , β and μ (parameters from Eq. 14), together with the statistical parameters R^2 and $RMSE$, for various different simulated values of soil moisture, incidence angle and polarisation.

Configuration		α	β	μ	R^2	RMSE (dB)
$M_v=10\%$	HH-20°	-16.14	12.34	23.71	0.86	1.44
	VV-20°	-15.11	10.21	38.31	0.77	1.53
	HH-40°	-24.19	18.13	11.27	0.93	1.57
	VV-40°	-20.71	15.10	14.02	0.90	1.63
$M_v=20\%$	HH-20°	-14.15	12.11	22.81	0.88	1.37
	VV-20°	-12.54	10.68	33.41	0.84	1.31
	HH-40°	-22.57	17.87	11.28	0.92	1.66
	VV-40°	-21.04	15.46	15.48	0.89	1.72
$M_v=30\%$	HH-20°	-13.05	12.01	22.95	0.87	1.35
	VV-20°	-11.09	10.86	32.26	0.86	1.24
	HH-40°	-22	-17.21	13.43	0.92	1.64
	VV-40°	-17.01	-14.92	17.65	0.92	1.34

Table 3: Radar satellite configurations corresponding to the radar data acquisitions, for the three studied sites.

Campaign	Sensor	date	Configuration
Orgeval'94	SIRC	12/04/94 - 18/04/94	C band, HH, 44°
Pays de Caux'94	ERASME	February 1994	C and X bands, HH, VV 20°, 25°, 30°, 35°
Villamblain'03	ASAR/ENVISAT	October 2003	C band, HH, ~43°

Table 4: Values of $\alpha_{p\theta}$, $\beta_{p\theta}$ and $\mu_{p\theta}$ (parameters of Eq. 15) together with the statistical parameters R^2 and $RMSE$, for the nine configurations analysed in this study.

	$\alpha_{p\theta}$	$\beta_{p\theta}$	$\mu_{p\theta}$	R^2	$RMSE$ (dB)
HH-20°	-14.11	12.63	35.95	0.77	1.29
VV-20°	-12.41	12.22	32.16	0.83	1.16
HH-25°	-12.85	10.91	22.45	0.76	1.4
VV-25°	-12.61	11.55	21.03	0.85	1.1
HH-30°	-12.68	10.08	15.68	0.76	1.38
VV-30°	-11.98	10.11	11.32	0.75	1.45
HH-35°	-12.56	9.41	12.05	0.7	1.54
VV-35°	-12.88	10.14	11.72	0.86	1.02
HH-44°	-10.28	5.63	4.62	0.7	0.89

Table 5: The statistical parameters R^2 and $RMSE$, corresponding to the use of different relationships between the radar data and the parameters kZ_s and kZ_g .

	kZ_s		kZ_g	
	R^2	$RMSE$ (dB)	R^2	$RMSE$ (dB)
HH-20°	0.67	1.5	0.77	1.29
VV-20°	0.79	1.21	0.83	1.16
HH-25°	0.65	1.69	0.76	1.4
VV-25°	0.77	1.39	0.85	1.1
HH-30°	0.67	1.6	0.76	1.38
VV-30°	0.67	1.69	0.75	1.45
HH-35°	0.65	1.66	0.7	1.54
VV-35°	0.8	1.2	0.86	1.02
HH-44°	0.86	0.6	0.71	0.86

Table 6: values of the parameters used in Eq. 16 for the HH and VV polarizations

	a_p	b_p	c_p	d_p	e_p	f_p	g_p
HH pol	0.046	-12.81	-0.026	10.55	0.05	-4.38	97.99
VV pol	-0.089	-9.88	-0.062	12.63	0.109	-7.346	134.61

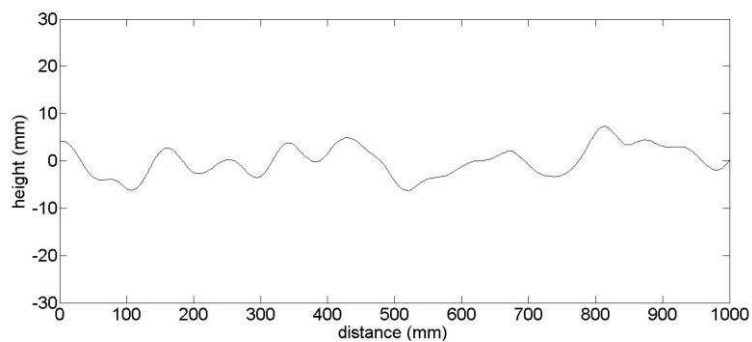
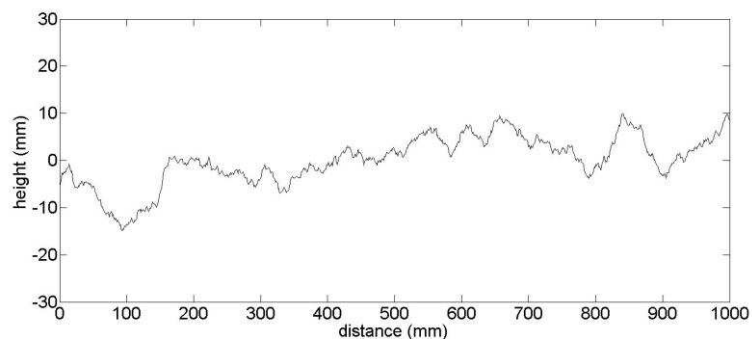
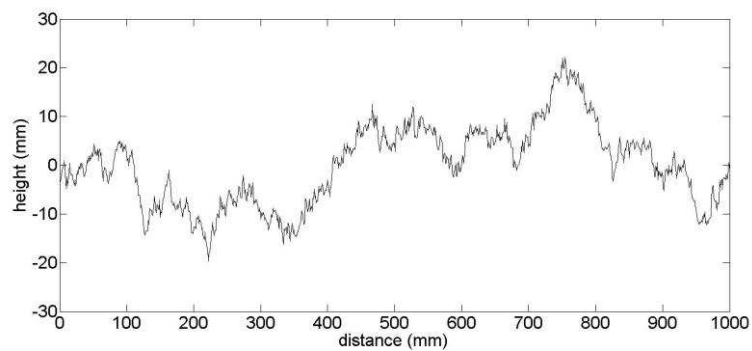
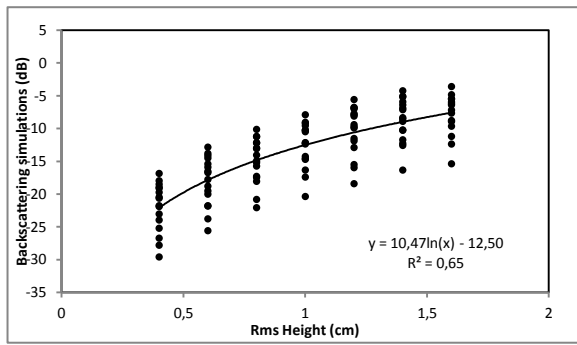
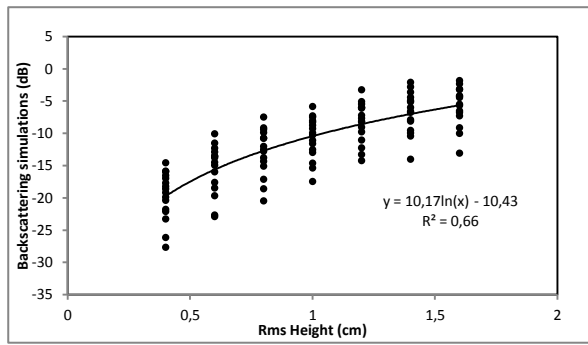


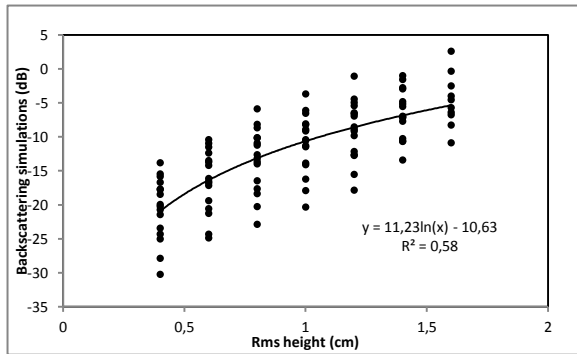
Fig. 1



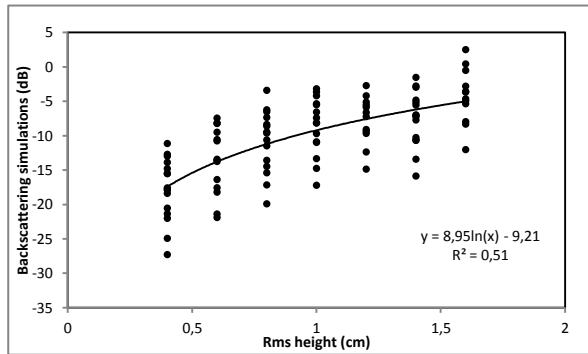
a)



b)

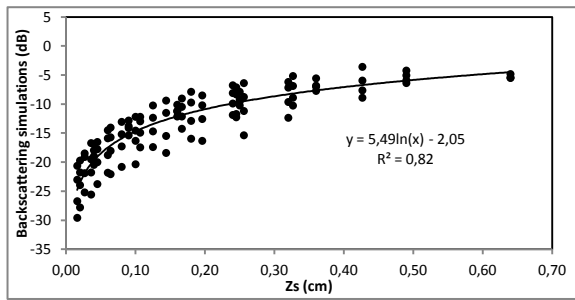


c)

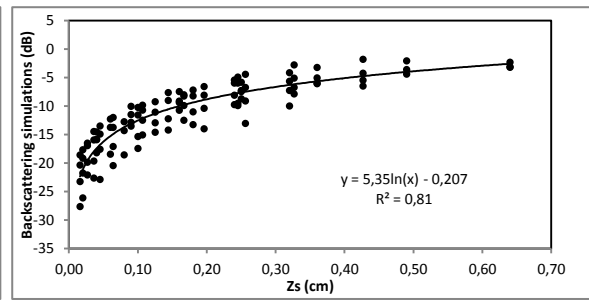


d)

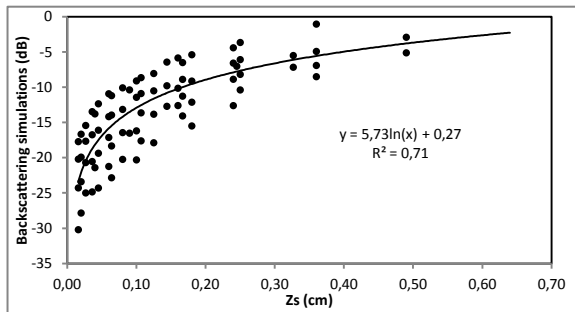
Fig. 2



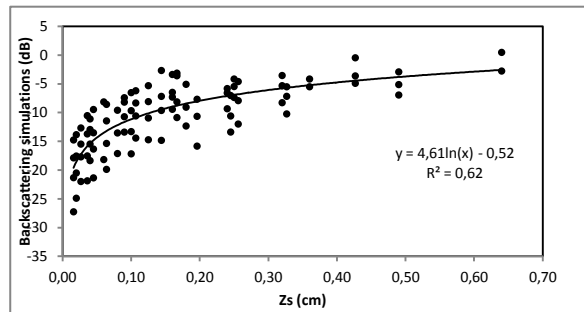
a)



b)



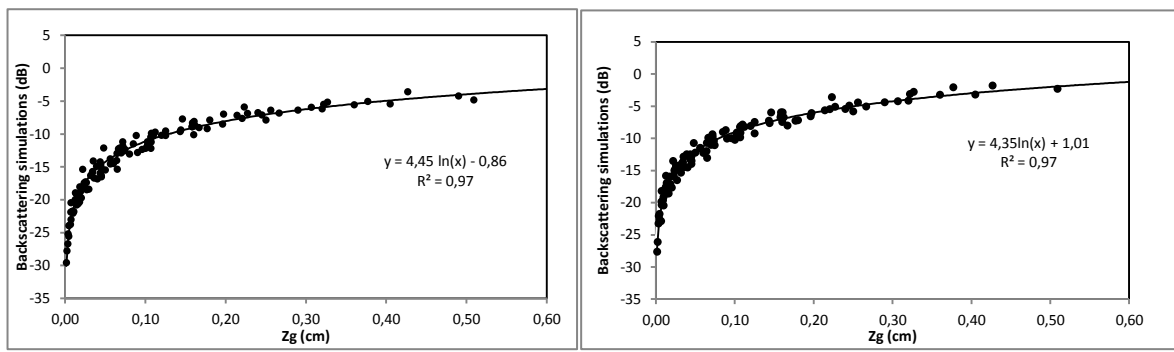
c)



d)

Fig. 3

576



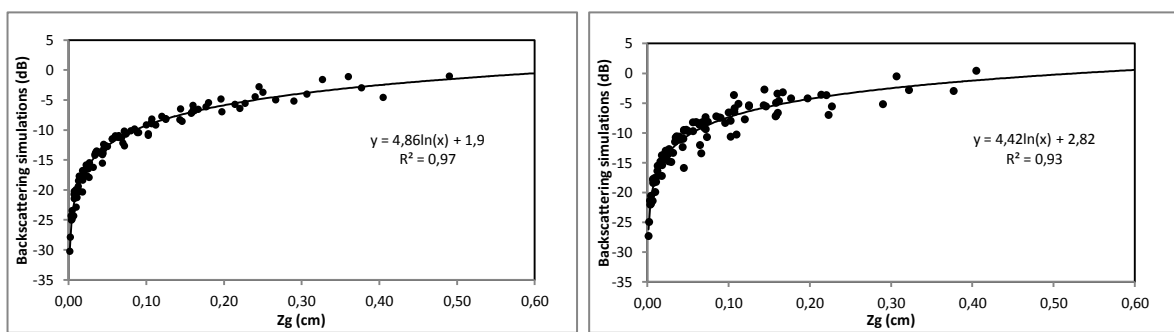
577

578

a)

b)

579



580

c)

d)

581 Fig. 4

582

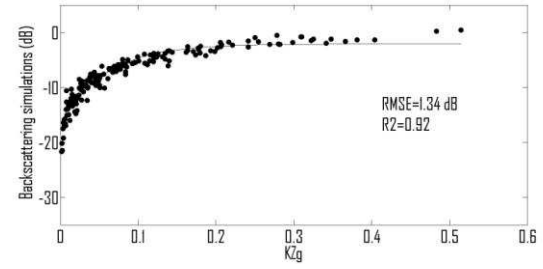
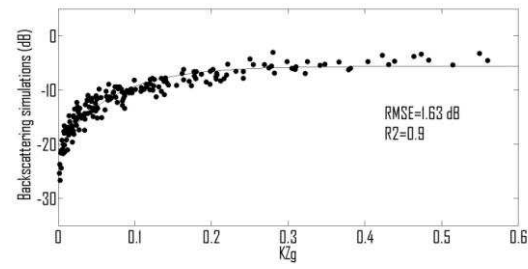
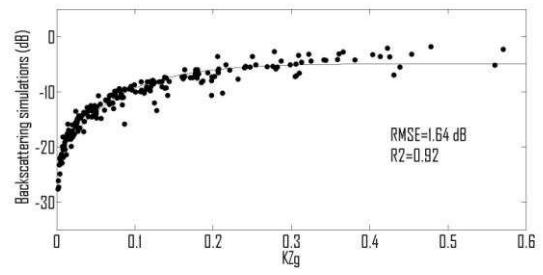
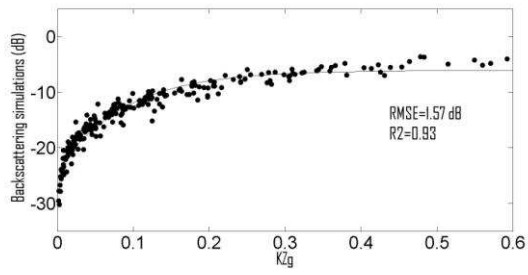
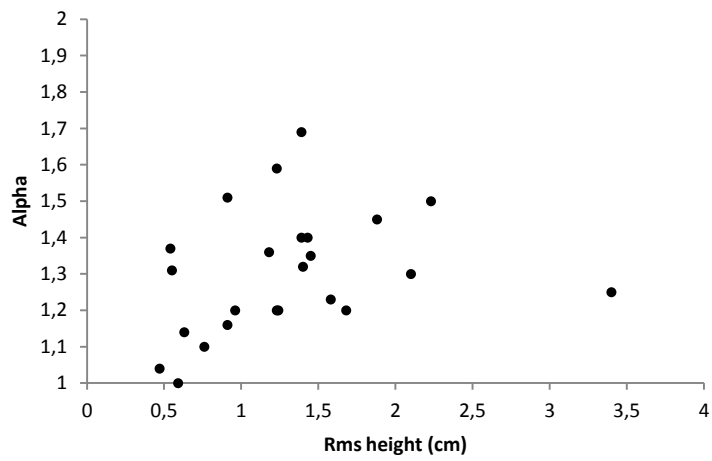


Fig. 5

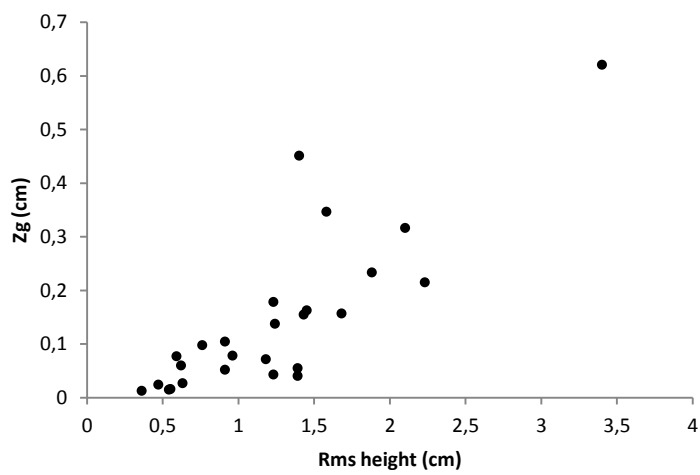


Fig. 6



596

597 (a)



598

599 (b)

600 Fig. 7

601

602

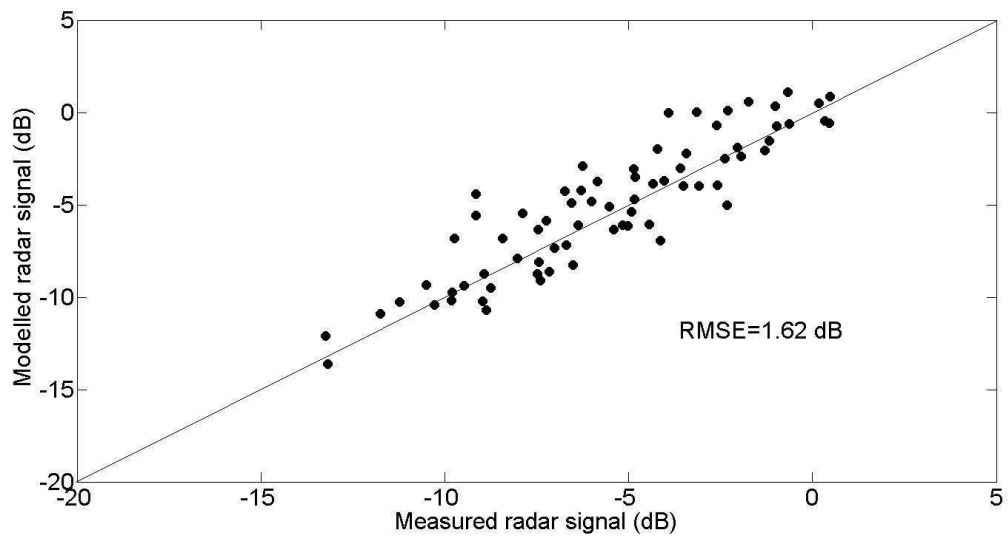
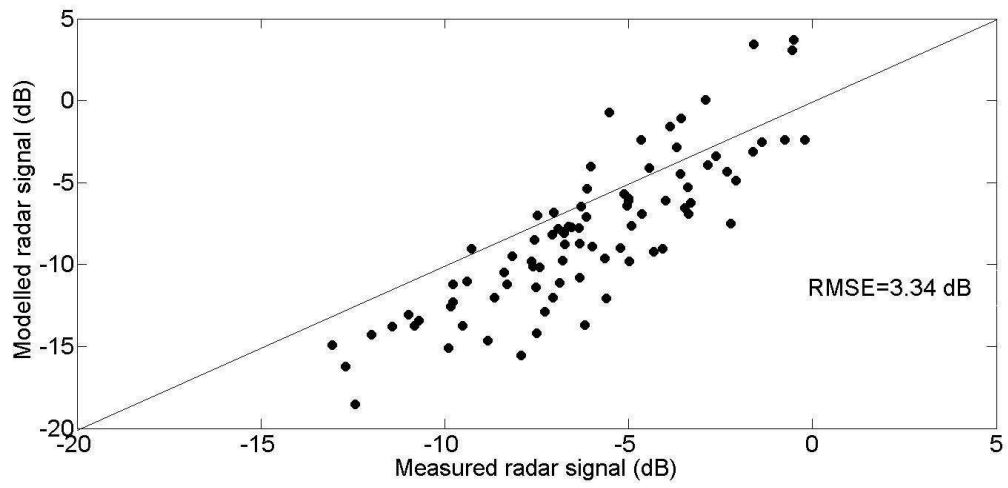
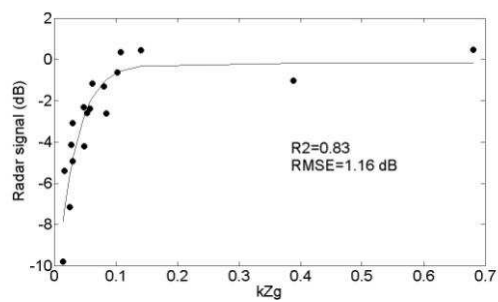
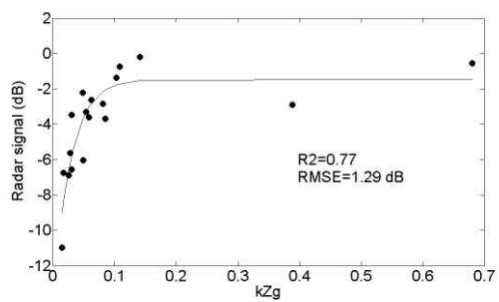
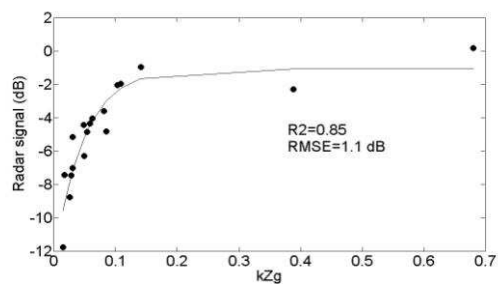
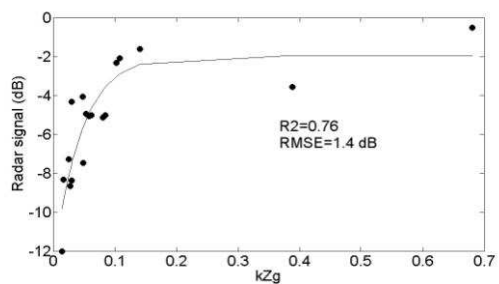


Fig. 8

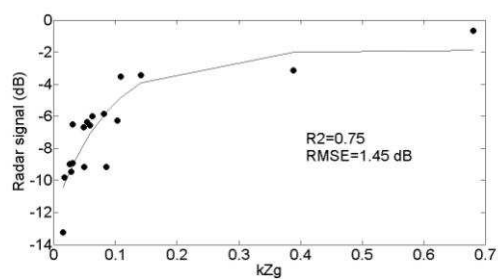
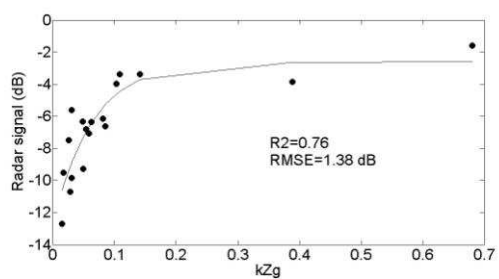
607



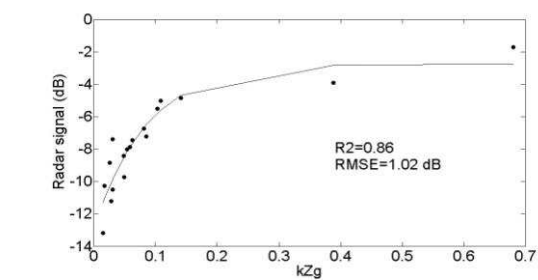
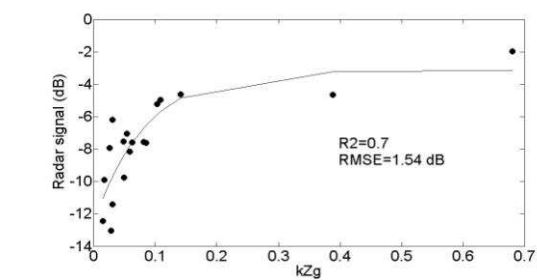
608



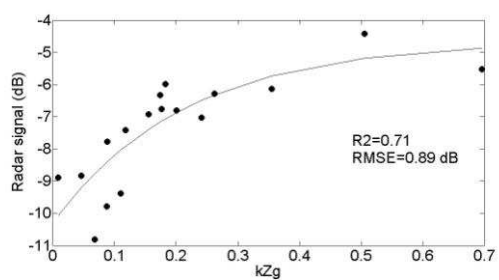
609



610



611



612

613

614 Fig. 9

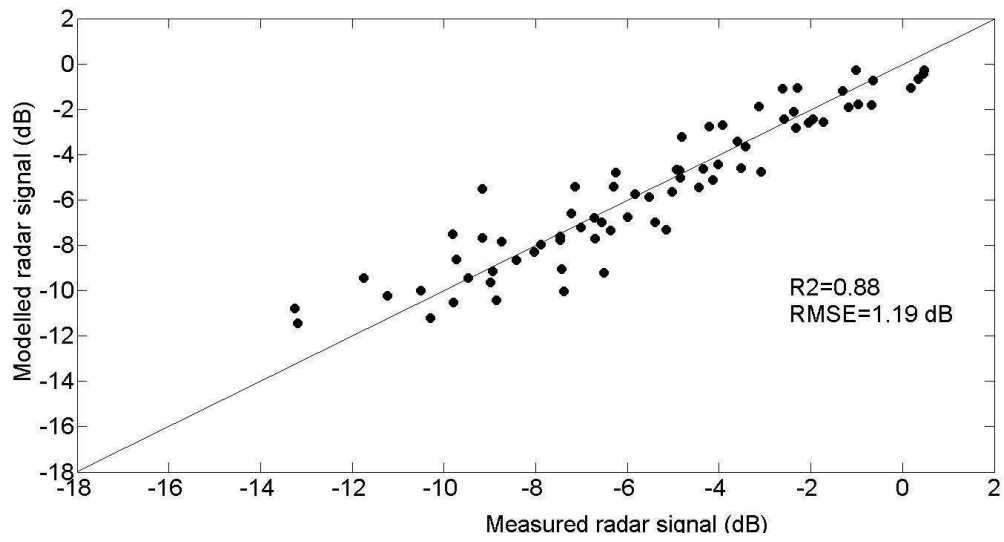
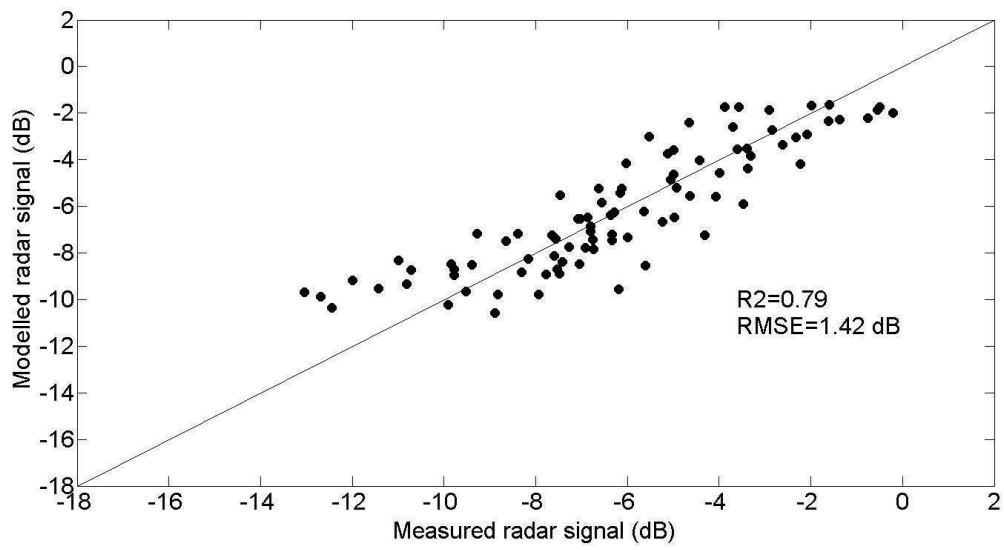


Fig. 10